

Coversheet

Title: Assessing and improving the robustness of Bayesian evidential learning in one dimension for inverting TDEM data: introducing a new threshold procedure

Authors Names:

Arsalan Ahmed^{1*} (arsalan.ahmed@ugent.be),

Lukas Aigner⁴ (lukas.aigner@geo.tuwien.ac.at),

Hadrien Michel⁵ (hadrien.michel@uliege.be),

Wouter Deleersnyder^{1,2} (wouter.deleersnyder@kuleuven.be),

David Dudal^{2,3} (david.dudal@kuleuven.be),

Adrian Flores Orozco⁴ (adrian.flores-orozco@geo.tuwien.ac.at),

Thomas Hermans^{1*} (thomas.hermans@ugent.be)

* Correspondence: arsalan.ahmed@ugent.be

Affiliation

¹ Ghent University, Department of Geology, Krijgslaan 281 - S8, 9000 Gent, Belgium

² KU Leuven Campus Kortrijk - KULAK, Department of Physics, Etienne Sabbelaan 53, 8500 Kortrijk, Belgium.

³ Ghent University, Department of Physics and Astronomy, Krijgslaan 281-S9, 9000 Gent, Belgium

⁴ Research Unit Geophysics, Department of Geodesy and Geoinformation, TU Wien, Vienna, Austria

⁵ University of Liege, Urban and Environmental Engineering Department, Faculty of Applied Sciences, Liege, Belgium.

"The paper is a non-peer-reviewed preprint that has been submitted to EarthArXiv. Subsequently, the preprint is submitted to the journal *Water*, which is published by MDPI."

Assessing and improving the robustness of Bayesian evidential learning in one dimension for inverting TDEM data: introducing a new threshold procedure

Arsalan Ahmed^{1*} <https://orcid.org/0000-0002-4893-2718>, Lukas Aigner⁴, Hadrien Michel⁵ <https://orcid.org/0000-0003-4960-449X>, Wouter Deleersnyder^{1,2} <https://orcid.org/0000-0003-4481-1801>, David Dudal^{2,3} <https://orcid.org/0000-0003-1326-6011>, Adrian Flores Orozco⁴ <https://orcid.org/0000-0003-0905-3718>, and Thomas Hermans^{1*} <https://orcid.org/0000-0001-9522-1540>

¹ Ghent University, Department of Geology, Krijgslaan 281 - S8, 9000 Gent, Belgium

² KU Leuven Campus Kortrijk - KULAK, Department of Physics, Etienne Sabbelaan 53, 8500 Kortrijk, Belgium.

³ Ghent University, Department of Physics and Astronomy, Krijgslaan 281-S9, 9000 Gent, Belgium

⁴ Research Unit Geophysics, Department of Geodesy and Geoinformation, TU Wien, Vienna, Austria

⁵ University of Liege ,Urban and Environmental Engineering Department, Faculty of Applied Sciences, Liege, Belgium.

Abstract: Understanding the subsurface is of prime importance for many geological and hydrogeological applications. Geophysical methods offer an economical alternative for investigating the subsurface compared to costly borehole investigation methods, but geophysical results are commonly obtained through an inversion whose solution is non-unique. Deterministic inversions providing a unique solution are computationally efficient while stochastic inversions investigating the full uncertainty range are more expensive. In this research, we investigate the robustness of the recently introduced Bayesian evidential learning in one dimension (BEL1D) to stochastically invert time domain electromagnetic data (TDEM). In particular, we analyse the performance and accuracy of BEL1D when using the coarser discretization used for the computation of the forward solution using SimPEG. We demonstrate that it is possible to speed-up BEL1D by introducing a threshold rejection method on the data misfit to by-pass iterations. In addition, we discuss the impact of the prior model space on the results. Finally, we apply the algorithm on field data collected in the Luy river catchment (Vietnam) to delineate saltwater intrusions. Our results show that the proper selection of timesteps and space discretization is essential to limit the computational cost while maintaining the accuracy of the posterior estimation. The selection of the prior distribution has a direct impact on fitting the observed data and is crucial to a realistic uncertainty quantification. The application of BEL1D for stochastic TDEM inversion is an efficient approach as it allows us to estimate the uncertainty at a limited cost.

Keywords: Uncertainty, Saltwater intrusion, TDEM, BEL1D, SimPEG

1. Introduction

Geophysical methods offer an economical alternative for investigating the subsurface compared to the use of direct methods. Most geophysical methods rely on a forward model to link the underlying physical properties (e.g., density, seismic velocity, or electrical conductivity) to the measured data and by solving an inverse problem. Deterministic inversions typically use a regularization approach to stabilize the inversion and resolve the non-uniqueness of the solution, yielding a single solution. However uncertainty quantification is generally limited to linear noise propagation [1,2,3,4]. In contrast, stochastic inversion methods based on a Bayesian framework compute an ensemble of models fitting the data, based on the exploration of the prior model space [5]. Although the increase of computer performance has advanced the use of stochastic approaches, long computational time remains an important issue for their broader adoption [6,7,8,9]. Indeed, most stochastic approaches rely on Markov chain Monte Carlo (MCMC) methods for sampling the posterior model space [5], which require a large number of iterations and forward model computations.

Alternatives have been developed to estimate the posterior distribution at a limited cost such as Kalman ensemble generators [10,11] or Bayesian Evidential learning (BEL) [12,13,14]. BEL has been recently proposed as an efficient alternative for the 1D inversion of geophysical data (BEL1D) [13,14]. BEL1D circumvents the inversion process by using a machine learning approach derived from Monte Carlo sampling of the prior distribution. It has been proven efficient for the estimation of the posterior distribution of water content and relaxation time from nuclear magnetic resonance data [13,15] and the derivation of seismic velocity models from the analysis of the dispersion curve [14]. The main advantage of BEL1D is to rely on a smaller number of forward model runs than MCMC approaches to derive the posterior distribution, leading to a reduced computational effort. Earlier work has shown that BEL1D converges towards the solution obtained from an MCMC procedure but it slightly overestimates the uncertainty, especially in case of large prior uncertainty [13]. The use of iterative prior resampling followed by a filtering of models based on their likelihood has been recently proposed to avoid uncertainty overestimation [14]. Although this increases the computational cost of BEL1D, it remains about one order of magnitude faster than MCMC [14].

So far, BEL1D has only been applied to a limited number of geophysical methods. In this contribution, we apply the algorithm to the inversion of time-domain electromagnetic (TDEM) data. We combine BEL1D with the TDEM forward modeling capabilities of the open-source Python package SimPEG [16] to stochastically solve the TDEM inverse problem. In the last decades, the popularity of TDEM has largely increased with the adoption of airborne TDEM surveys for mineral but also hydrogeological applications (e.g., [17,18,19]). More recently, towed transient electromagnetic (tTEM) systems [20] and waterborne TEM systems [21,22,23], are designed for continuous measurements of TEM data; thus, allowing to cover large areas in relatively short times.

To date, the inversion of such extensive surveys rely on deterministic quasi-2D or -3D inversion [24], i.e. using a 1D forward model with or without lateral constraints.

Stochastic approaches for the inversion of TDEM are still rare (e.g. [7,9]), yet these are computationally demanding for large data sets, as the whole inversion needs to be re-run for every sounding independently. Hence, developing a fast alternative is highly relevant for to-date hydro geophysical investigations.

In this paper, we focus on the ability of BEL1D to retrieve the posterior distributions of electrical subsurface model parameters from the inversion of TDEM data. We explore the convergence and resolution of the stochastic inversion as well as the computational time, by varying the temporal and spatial discretization of the forward solver. We also discuss the selection of the prior model. We apply this approach to TDEM data collected in the Luy river catchment in the Binh Thuan province (Vietnam) for saltwater intrusion characterization.. In this study, we use the pyBEL1D package proposed by [25] for all calculations.

2. Materials and Methods

2.1. BEL1D

In contrast to deterministic approaches, BEL1D does not rely on the stabilization of the ill-posed inverse problem through regularization. Instead, BEL1D learns a statistical relationship between the target (the set of parameters of interest, in this case a subsurface layered model of the electrical conductivity) and the predictor (the geophysical data). This statistical relationship is derived from a combination of models and data (typically a few thousand) drawn from the prior distribution which reflects the prior geological knowledge. For each sampled model, the forward model is then run to generate the corresponding data set [13] Next, a statistical relationship is learned in a lower dimensional space and used to calculate the posterior distribution corresponding to any data set consistent with the prior, without the need to run any new forward model. We refer to [13,14] for details about the algorithm. Here, we only provide a short overview. BEL1D consists of seven steps:

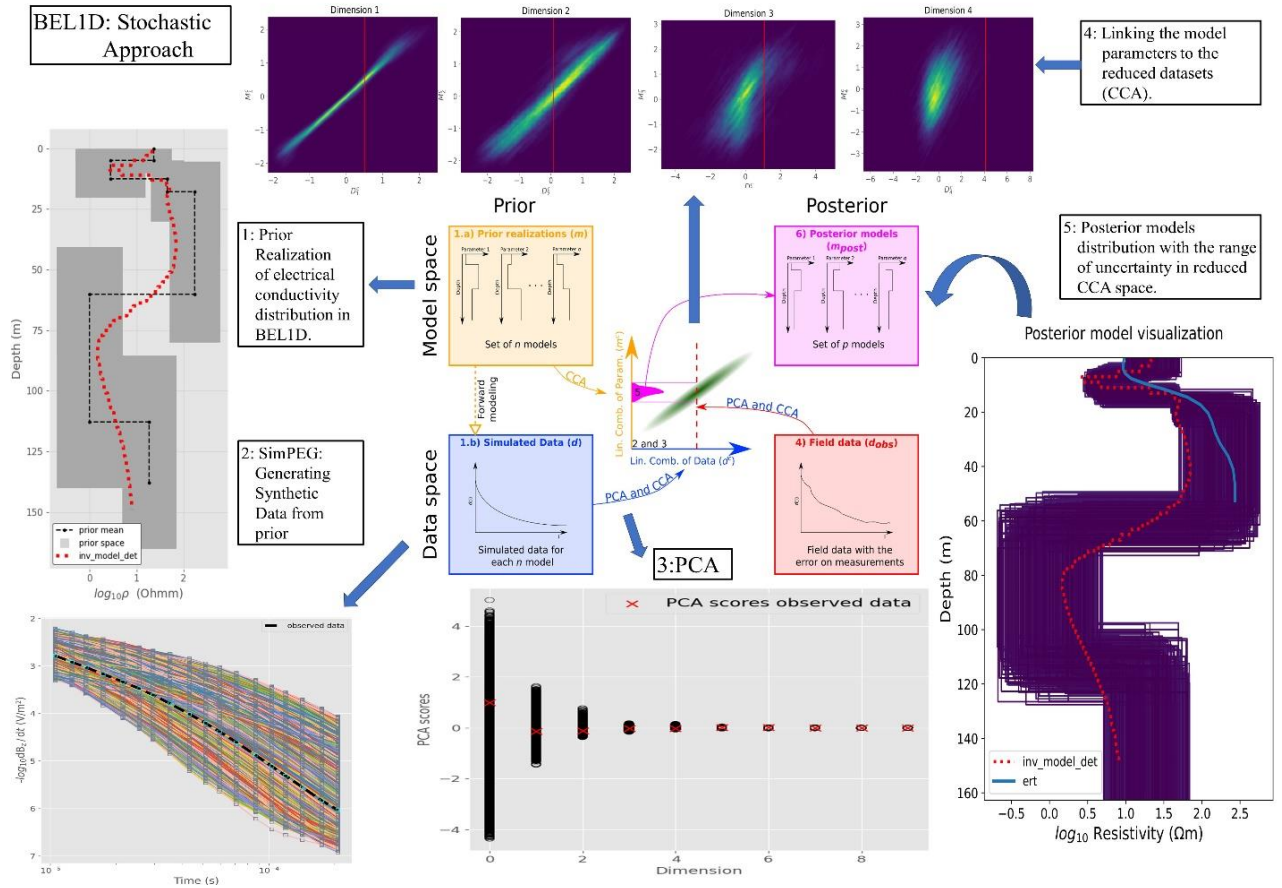


Figure 1: The schematic diagram of BEL1D applied to TDEM data (modified from [15])

Step 1: Prior sampling and forward modeling

As in any stochastic inversion, the first step is to assign the range of prior uncertainty based on earlier field knowledge. For TDEM 1D inversion, we need to define the number of layers, their thickness and electrical conductivity. A set of n prior models is sampled. For each sampled model, the corresponding TDEM data are simulated using the forward model. In this step, it is important to state the size of the transmitting and receiving loop, the waveform and magnetic momentum of the primary field as well as the acquisition time and sampling of the decay-curve.

More specifically, this first step entails defining the prior model using a finite set of N_L layers, with the final layer simulating the half-space. Except for this layer, which is defined by its conductivity only, the other layers are defined by their conductivity and thickness. Thus, the total number of model parameters or unknowns is $q = 2 \times N_L - 1$. For each of those q parameters, a prior distribution is described, which must reflect the prior understanding of the survey site. Such information can be based on either previous experiments or more general geological and geophysical

considerations. Random models are sampled within the prior range, and the forward model is run for each one to calculate the corresponding noise free data set \mathbf{d} (Figure 1, boxes 1 and 2):

$$\mathbf{d} = \mathbf{f}(\mathbf{m})$$

where \mathbf{m} is the set of q model parameters and \mathbf{f} is the forward model solving the physics (see section 2.2)

Step 2: Reducing the dimensionality of data.

Lowering the dimensionality of the data is required to determine a statistical connection between the target and the predictor. Dimension reduction also helps to limit the impact of noise on the inversion [26]. Principal component analysis (PCA) identifies linear combinations of variables that explain most of the variability by using the eigenvalue decomposition [27]. Higher dimensions typically exhibit less variability and can be disregarded. Noise is propagated using Monte Carlo simulation [13,26] to estimate the uncertainties of the PCA scores caused by data noise (Figure 1 box 3). Similarly, the dimensions of model parameters q can be reduced if necessary.

Step 3: Statistical relationship between target (model parameters) and predictor (the reduced dataset)

Canonical correlation analysis (CCA) is used to determine a direct correlation between the target and predictor [13]. CCA essentially calculates the linear combinations of (reduced) predictor variables and target variables that maximize their correlation, producing a set of orthogonal bivariate relationships [27]. The correlation typically decreases with the dimensions, the first dimension being the most correlated (Figure 1 box 4). Step 4: Generation of the posterior distributions in CCA space.

In the CCA reduced space, kernel density estimation (KDE) with a Gaussian kernel [28] is used to map the joint distribution $f_H(\mathbf{m}_c, \mathbf{d}_c)$ where the suffix c refer to the canonical space and m and d stands for model and data . We employ a multi-Gaussian kernel with bandwidths selected in accordance with the point density [13]. The resulting distributions are not restricted to any specific distribution with a predetermined shape. As a result, a simple and useful statistical description of the bivariate distribution can be generated (Figure 1 box 4).

Step 5: Sampling of the constituted distributions

The KDE maps are then used to extract the posterior distribution $f_H(\mathbf{m}_c | \mathbf{d}_{obs,c})$ for any observed data set projected into the canonical space $\mathbf{d}_{obs,c}$ using the inverse transform sampling method [29] We can now easily generate a set of samples from the posterior distributions in the reduced sample (Figure 1 box 5).

Step 6: Back transformation into the original space.

The set of the posterior samples in CCA space are back transformed into the original model space. The only restriction is that more dimensions must be kept in the predictor than the target in order to support this back transformation. The forward model is then run for all sampled models to compute the root-mean-squared error (RMSE) between observed and simulated data.

Step 7: Refining the posterior distribution by IPR with threshold

In case of large prior uncertainty [14], recommend applying iterative prior resampling (BEL1D-IPR). The idea is to enhance the statistical relationship by sampling more models in the vicinity of the solution. In short, models of the posterior distribution are added to the prior distributions, and steps 2 to 6 are repeated. This iterative procedure is followed by a filtering of the posterior models based on their likelihood using a Metropolis sampler. This allows to sample the posterior distribution more accurately but at a larger computational cost.

Here, we propose to reduce the computational effort by applying a filtering procedure after the first iteration. The threshold criterion is defined based on the expected RMSE (rRMSE) estimated from the data noise. The rRMSE is calculated in log space to account for the large range of variations in the amplitude of the measured TDEM signal, so that a systematic relative error expressed in % corresponds to a predictable value of the rRMSE calculated in log space. With such an approach deviating from the Bayesian framework, the posterior solution is only an approximation of the true posterior distribution. The main advantage is to eliminate the need to run new forwards models and to ensure that the same prior distribution can be used for several similar data sets, making the prediction of the posterior very fast in surveys with multiple soundings. We refer to this new approach as BEL1D-T.

2.2. SimPEG: Forward Solver

We use the open-source python package SimPEG to obtain the TDEM response for a given set of model parameters and acquisition set-up [16]. The main advantage of SimPEG is that it provides an open source and modular framework, for simulating and inverting many types of geophysical data. We opted for a numerical implementation instead of the more classical semi-analytical solution such as the one provided in `empymod` [30] to assess the impact of an error in the forward model on the estimation of the posterior. We limit ourselves to a strictly 1D context, yet the approach could be extended to assess the error introduced by multi-dimensional effects (through a 2D or 3D model), and is therefore more flexible. However, the use of a 3D model increases the computational cost and it is beyond the scope of this study to compare numerical and semi-analytical forward solvers.

The SimPEG implementation uses a staggered grid discretization [31] for the finite volume approach [32], which calls for the definition of the physical properties, fields,

fluxes, and sources on a mesh [33,34,35]. The details of the implementation can be found in [32] and [16] For the 1D problem, SimPEG makes use of a cylindrical grid. The accuracy and computational cost of the forward solver depend on the time and space discretization.

2.2.1. Temporal discretization

For the temporal discretization, it is a good practice to start with short time steps at the early times when the electromagnetic fields change rapidly [41]. At later stages, the time steps can be increased as the variations in the EM fields are more gradual and the signal-to-noise ratio (S/N) decreases. Shorter time steps increase the accuracy of the forward model but also the calculation time. Hence, it is important to find an adequate trade-off between accuracy and computational cost. In this paper, we tested three sets of temporal discretization with increased minimum and average size for the time-steps (Table1 and Figure 2).

Table1 : Description of the different temporal discretization. F (fine), I (intermediate) and C (coarse) are the corresponding acronyms.

Temporal Discretization	Total Number of Time steps	Maximum size of time steps (sec)	Weighted average length of time Steps (sec)
Fine (F)	1710	10^{-5}	0.581×10^{-6}
Intermediate (I)	510	10^{-5}	1.95×10^{-6}
Coarser (C)	185	10^{-4}	5.38×10^{-6}

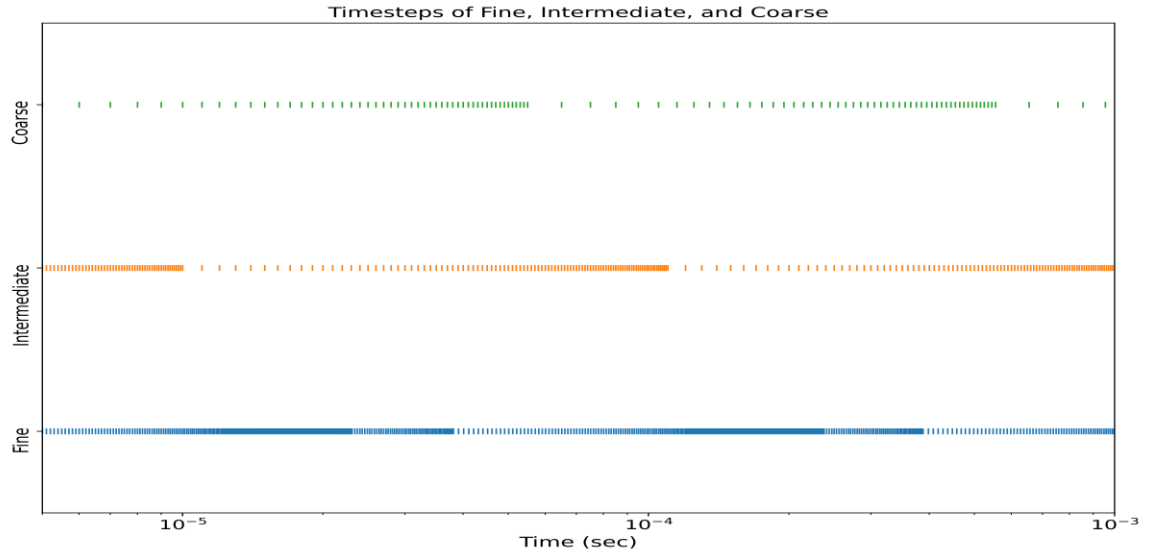


Figure 2 : Visual representation of the time discretization. The Y-axis shows the time discretization and the X-axis shows the logarithmic scale of the time steps size.

2.2.2. Spatial discretization

Spatial discretization also has a direct impact on the accuracy of the forward solver. When creating the mesh as shown in figure 3, the discretization in the vertical direction is controlled by the cell size in z-direction, whereas the horizontal discretization is controlled by the cell size in x-direction. A finer discretization results in a more accurate solution but is also more computationally demanding. Note that a coarse discretization might also prevent an accurate representation of the layer boundaries as defined in the prior. If the layer boundary does not correspond to the edge of the mesh, a linear interpolation is used. In this paper, we selected five values for the vertical discretization to test the impact of the spatial discretization on the estimated posterior (Table 2).

Table 2: Cell size in z-direction for the different spatial discretization. The letters in brackets VF (very fine), F (fine), M (medium), C (coarse) and VC (very coarse) are used as acronyms in the remaining of this paper.

Spatial Discretization	Thickness of grid cells (in m)
Very Fine (VF)	0.25
Fine (F)	0.5
Medium (M)	1
Coarse (C)	1.5
Very Coarse (VC)	2

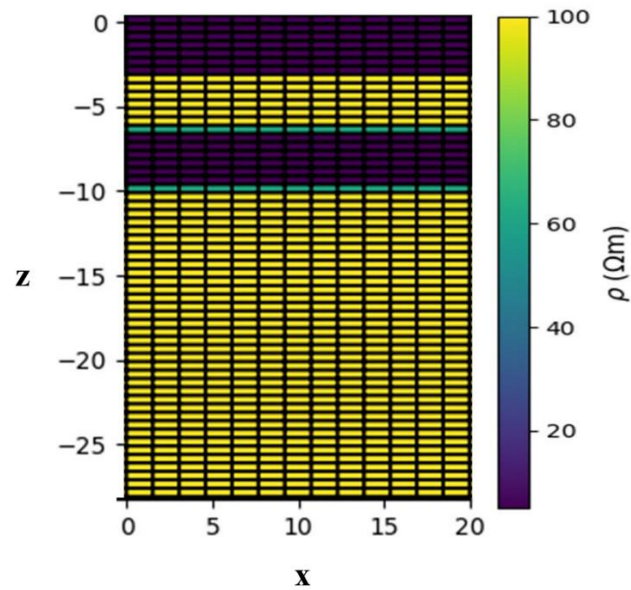


Figure 3. Example of the cylindrical mesh used for the forward model with a vertical discretization of 0.5 m, and a horizontal discretization of 1.5 m. The cells with positive z, represent the air and are modelled with a very high resistivity and logarithmically increasing cell size.

2.3. Synthetic benchmark

We analyzed the impact of both temporal and spatial discretization on the accuracy of the posterior distribution, for all fifteen combinations of the temporal and spatial discretization (see Table 1 and Table 2) using synthetic data. A single combination is referred to by its acronyms, starting with the time discretization. The combination F-C for example corresponds to the fine time discretization combined with the coarse spatial discretization.

The synthetic data set is created with the finest discretization using the benchmark model parameters in brackets (see Table 3) defined by a five-layer model, with the last layer having an infinite thickness. The prior is also the same for all tests and consists of uniform distributions for the 9 nine model parameters (Table 3). The acquisition settings mimic the field set-up; see the following subsection.

Table 3: Prior range of values for all parameters of the model. Benchmark model parameter for the synthetic model are shown in brackets.

Layers	Thickness (m)	Resistivities (ohmm)
Layer 1	0.5 -6.5 (5)	10-55 (20)
Layer 2	5 – 15 (10)	1-15 (4.5)
Layer 3	0.5 – 10 (5)	20-100 (50)
Layer 4	35 – 50 (42)	50-115 (75)
Layer 5	∞ (∞)	5-20 (10)

3. Field Site

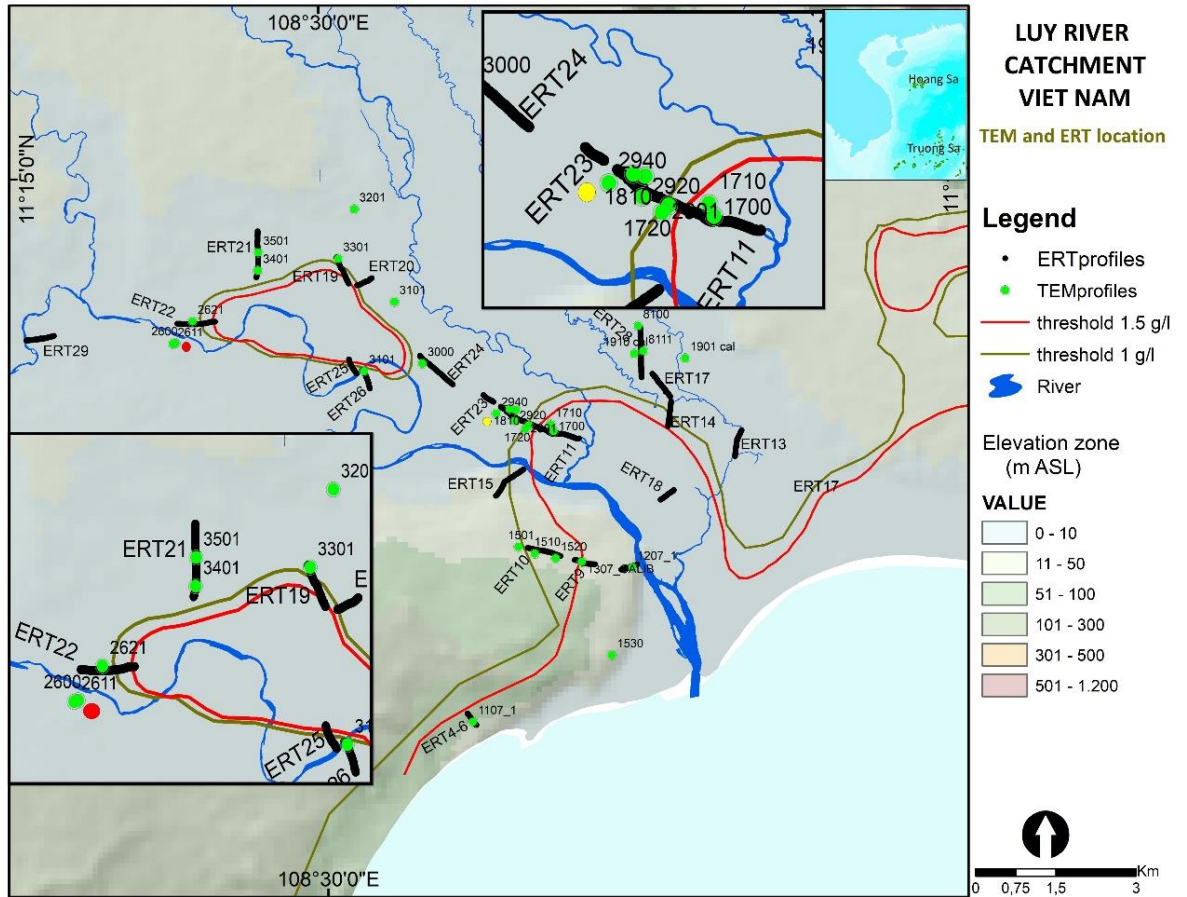


Figure 4: The Luy river catchment in Vietnam with location of TDEM soundings (green points) and ERT profile (black line). The red and yellow dots represent the location of the soundings (2611 and 1307) used in this paper [36,37].

Understanding the interactions between salt and freshwater dynamics is crucial but difficult for managing coastal aquifers (e.g., [38,39]). The study area for the field tests is located in the Luy River catchment in the Binh Thuan province (Vietnam), which has been facing saltwater intrusions problems for many years [36,37].

The data were collected using the TEM- FAST 48 equipment, with a 25 m square loop with a single turn acting as both transmitter and receiver. The injected current was set to 3.3A with a dead-time of 5 μ s. The data were collected using 42 semi-logarithmic time windows ranging from 4 μ s to 4 ms. The signal was stacked allowing for noise estimation. A 50Hz filter was applied to remove noise from the electricity network. For the inversion, the early time and late time were manually removed (see Figure 11). The recorded signal at early time step, i.e below 10⁻⁵ μ s were

impacted by the current switch off phenomena while above 1 ms, the signal-to-noise ratio is too low. We therefore filtered the TEM data to a time range from 8 μ s to 500 μ s. In the forward model, we implemented the current shut-off ramp from the TEM-FAST48 system following the approach proposed by Aigner et al. (2024).

4. Results

We subdivide the results in 4 subsections. In the first subsection, we analyze the impact of the accuracy of the forward solver on the accuracy of the posterior in BEL1D-IPR. In the second section, we test the impact of a threshold on the rRMSE applied after the first BEL1D iteration (BEL1D-T). The third subsection is dedicated to the selection of the prior. Finally, the last section corresponds to the application of BEL1D-T to field data.

4.1. Impact of Discretization

In this section, we tested in total 15 combinations of temporal and spatial discretization to study their behavior on both computational time and accuracy of the posterior distribution computed with BEL1D-IPR (4 iterations). The reference is using the finest time and spatial discretization (F-VF). Since the computational costs of BEL1D is directly related to the number of prior samples and the computational cost of running one forward model [25], computing the solution for the F-VF combination is more than 150 times more expensive than running it with the C-VC combination (Table 4). An initial set of 1000 models is used in the prior. All calculations and simulation were carried out on a desktop computer with the following specifications: Processor intel © CORE™ i7-9700 CPU @ 3.00 GHz, RAM 16.0GB.

Table 4: Time (in seconds) to solve one time the forward model in SimPEG for the 15 combination of time and special discretization. The red color corresponds to posterior distributions whose mean is biased whereas the blue color represents an under- or overestimation of the uncertainty for the two shallowest layers.

	Spatial Discretization				
Time	VF	F	M	C	VC
F	389.02	73.88	33.4	25.92	17.7
I	114.79	22.38	6.3	3.55	2.73
C	44.98	11.48	3.90	2.46	2.02

We first analyze the impact of the forward solver in BEL1D-IPR. A very similar behavior is noted for all combinations using the VF spatial discretization, in combination with the three temporal discretization for all parameters (Figure 5). The parameters (thickness and resistivity) of the two first layers are recovered with relatively low uncertainty, while the uncertainty remains quite large for deeper layers, showing the intrinsic uncertainty of the methods related to the non-unicity of the solution. The results look globally similar but a detailed analysis of the posterior distribution focusing on the resolved parameters (two first layers, see Figure 6) shows a slight bias of the mean value in C-VF and I-VF for the thickness of the second layer. This bias is small (less than 0.5 m) and could be the result of the sampling. A slightly larger uncertainty range can also be observed for the I and C time discretization.

Globally, a systematic bias is observed for the largest spatial discretization (VC and C) for the thickness of layers 1 and 2 (Figure 6), what can likely be attributed to the difficulty to properly represent thin layers with a coarse discretization. A bias in the thickness of layer 2 is also noted for all coarse time discretization, and to a lesser extent for the intermediate time discretization, although this is limited when combined with F and VF spatial discretization. There is no significant bias visible in the estimation of the resistivity of layer 1, while most combinations have a small but not significant bias for layer 2, and the uncertainty range tends to be overestimated or underestimated for most combinations with large spatial discretization. Eventually, combinations with a VF or F spatial discretization combined to all time discretization, as well as the F-M combination, provide relatively similar results to the reference F-VF.

The time and spatial discretization for simulating the forward response of TDEM have therefore a strong impact not only on the accuracy of the model response, but also on the estimation of the parameters of the shallow layers after inversion. In particular, the coarser spatial discretization biases the estimation of the thicknesses of the shallow layer. The same is also observed for the combination of a coarse or intermediate time discretization with a medium spatial discretization. As shallow layers correspond to the early times, this bias is likely related to an inaccurate simulation of the early TDEM response by the forward solver due to the chosen discretization. Although it comes with a high computation cost, we recommend to keep a relatively fine time and space discretization to guarantee the accuracy of the inversion. The cheapest option in terms of computational time with a minimum impact on the posterior distribution corresponds in this case to the C-F combination.

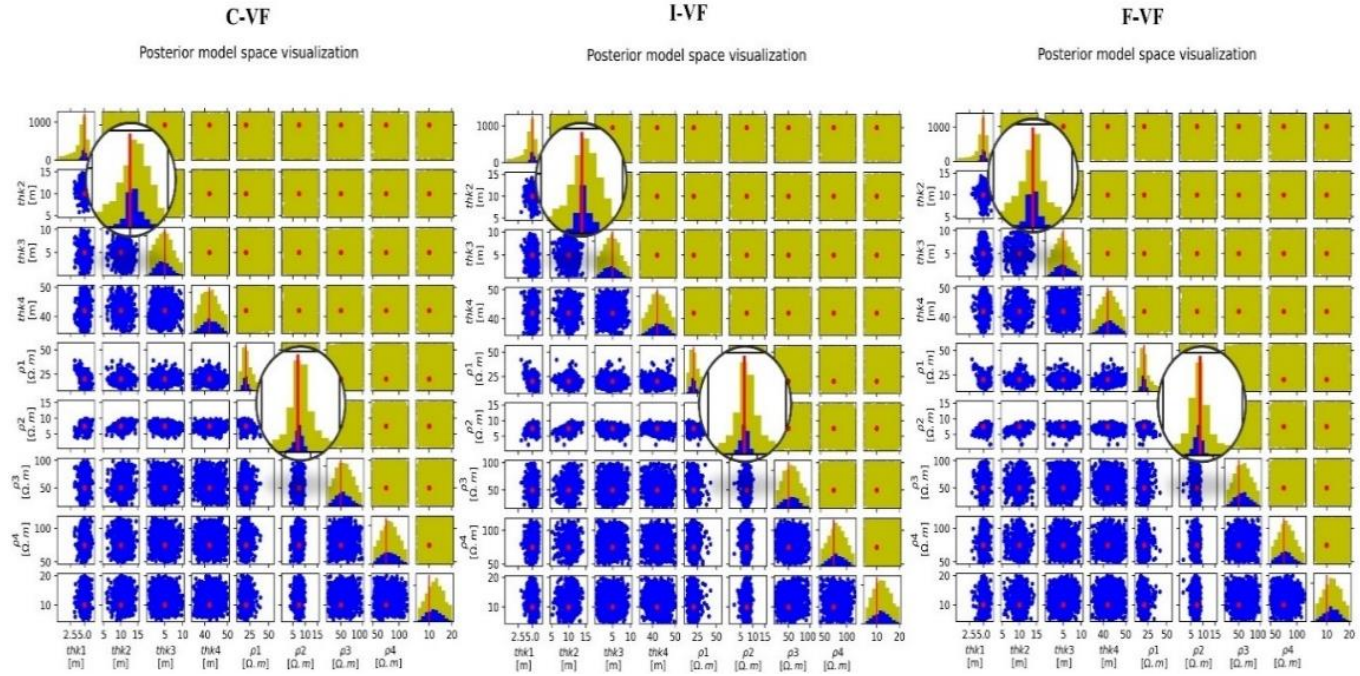


Figure 5: Posterior model space visualization of fine, intermediate and coarse time discretization with very fine spatial discretization symbolized as (C-VF, I-VF and F-VF).

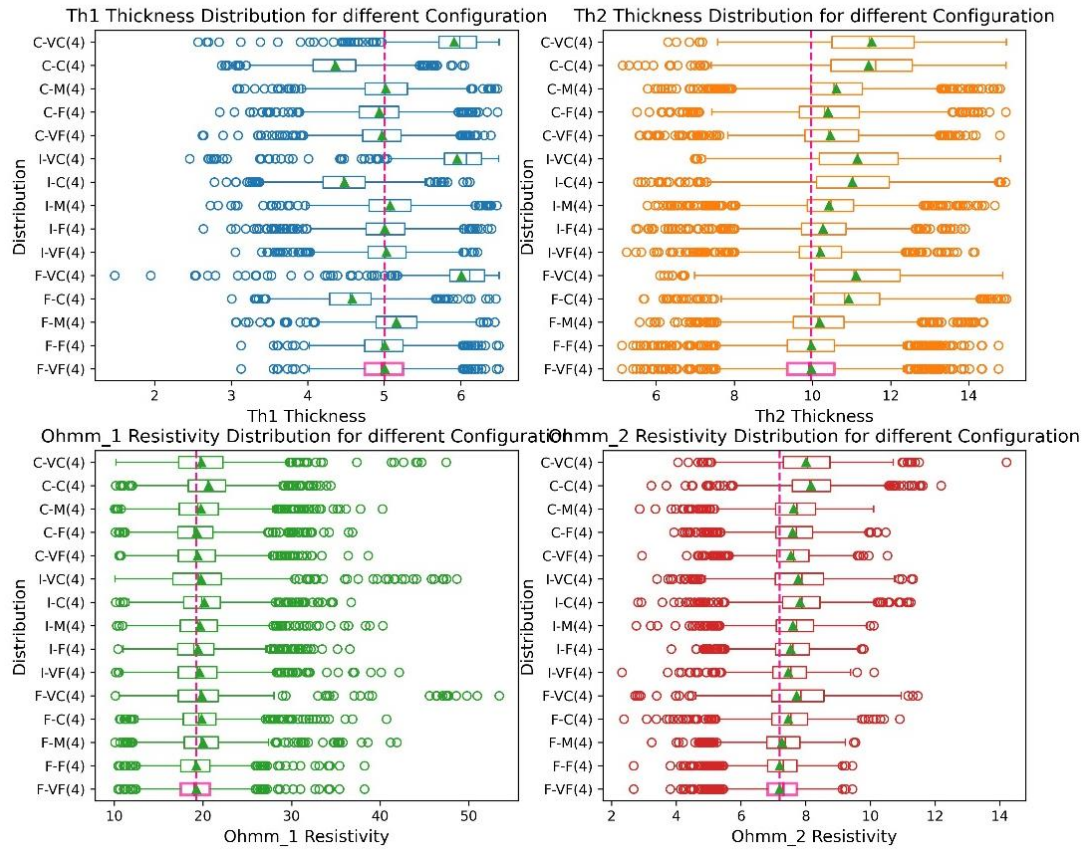


Figure 6 : Box plot of first two layers thickness and resistivity for BEL-IPR (4 iterations). The red line shows the benchmark value and the F-VF(4) is the reference solution.

4.2. Impact of the Threshold

Because of the additional costs associated with the iterations, we compare the posterior distributions obtained with BEL1D-IPR to our new BEL1D-T approach applying a threshold after the 1st iteration. The selected threshold based on the rRMSE calculated on the logarithm of the data are 0.18, 0.135, 0.05, corresponding respectively to a systematic error on the data of 20, 15 and 5%. Various values of the threshold are tested for the reference solution (F-VF discretization) (Figure 7) and the analysis of the discretization is repeated (Figure 8). The threshold is applied after the first iteration to avoid additional computational time. The corresponding posterior distribution retains only the models which fit the data to an acceptable level. Note that the corresponding posterior distributions has a lower number of models than the IPR on BEL1D as the latter enriches the posterior with iterations.

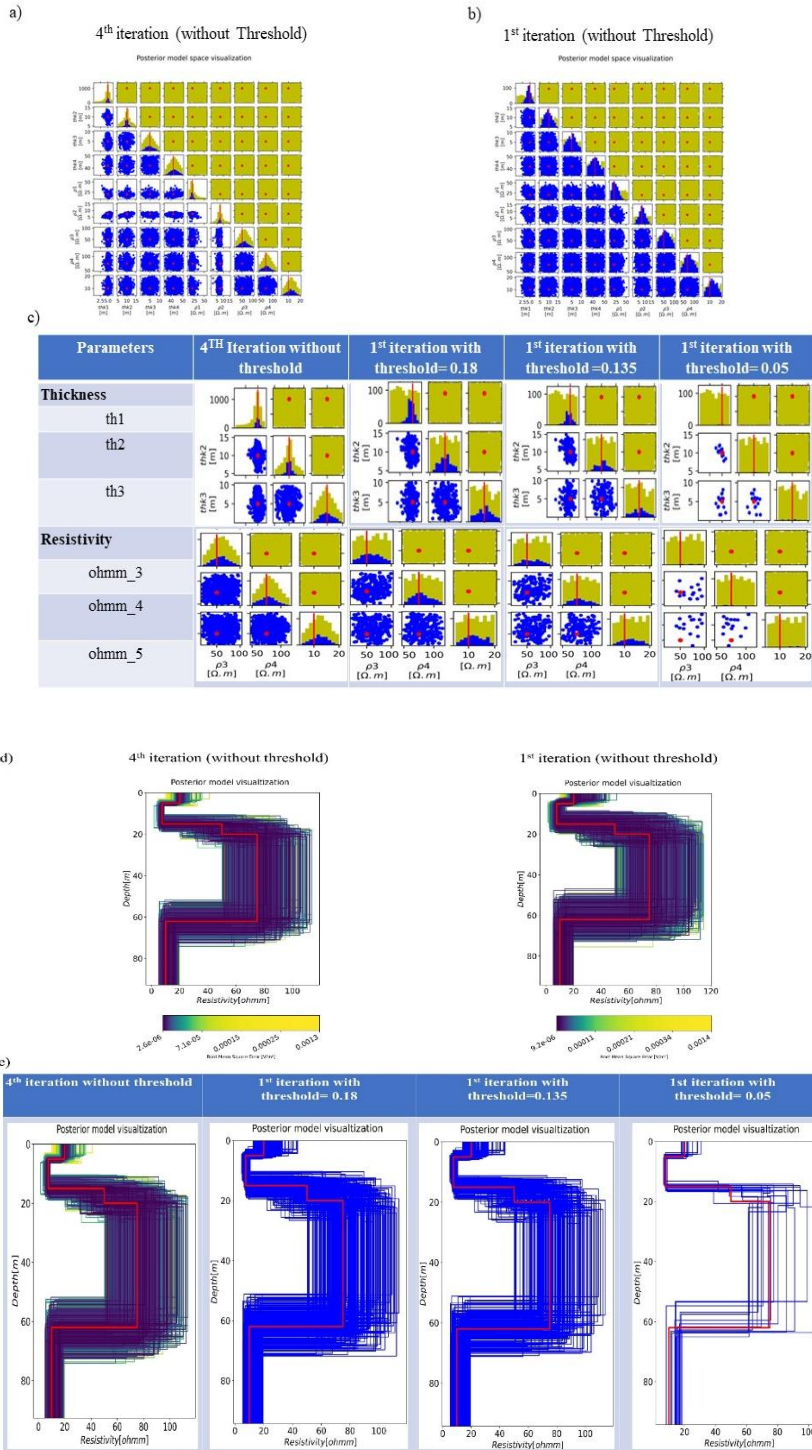


Figure 7: Posterior model space visualization: yellow dots represent the prior distribution, blue dots show the posterior distribution and the red line corresponds to the benchmark model. The panels represent: a) the posterior model space distribution at 4 iteration 4 without threshold (BEL1D-IPR), b) the posterior model space distribution at 1 iteration 1 without threshold application c) the comparison between BEL1D-IPR and with three threshold values for BEL1D-T (0.18, 0.135 and 0.05). The x- and y-axis are equivalent to resistivity (ohmm)

and depth (m)) Posterior model distribution for BEL1D-IPR (left) and after 1 iteration without threshold (right) e) Posterior model distribution for BEL1D-IPR and BEL1D-T with threshold values (0.18, 0.135 and 0.05).

For solutions without threshold, the color scale is based on the quantiles of the RMSE in the posterior distribution. The threshold thus removes the models with the largest RMSE (yellow-green).

Without the threshold (Figures 7a, 7b and 7d), some models not fitting the data are present in the posterior. The threshold approach after 1 iteration succeeds in obtaining a posterior closer to the reference solution (Figures 7c and 7e). The benchmark model, which is the true model, lays in the middle of the posterior.

The impact of the selected threshold value on the posterior distribution is illustrated in Figures 7c and 7e. Since the threshold is based on the rRMSE, decreasing its value is equivalent to reject the models with the largest data misfit from the posterior, while only models fitting the data with minimal variations are kept in the posterior. This rejection efficiently removes poor models from the posterior. If a low value is selected, only the very few best fitting models are kept, and these are very similar to the reference model, hence, reducing the posterior uncertainty range in the selected models. The choice of the threshold should therefore be carefully made based on the noise level.

For the selected threshold value of 0.135, only 166 models are retained after filtering, corresponding to a rejection rate of 83.4%. If more models are required in the posterior, it is necessary to generate new models, which is not computationally expensive in BEL1D. The only additional effort is to compute the resulting RMSE. The total computational effort is therefore proportional to the efficiency of the forward solver (Table 4). For instance, generating 500 models in the posterior would require to generate 3000 samples based on the same rejection rate, and therefore would take 3 times more time. BEL1D-T is therefore equivalent to a smart sampler that quickly generates models only in the vicinity of the posterior distribution and can contribute to a first fast assessment of the posterior. If the generation of many models is required, we rather recommend using BEL1D-IPR.

In this case, the threshold value of 0.135 seems acceptable and close to the BEL1D-IPR posterior distribution after 4 iterations. A higher threshold seems to retain too many samples resulting in an overestimation of the posterior. The threshold value of 0.05 corresponds to a very large rejection rate and would require to generate more models to assess the posterior properly. In the remaining part of the paper, the threshold 0.135 is used. The visualization of model space encompassing all combinations of temporal and spatial discretization for the first two layers' thicknesses is illustrated in Figure (A) of the supplementary material. Correspondingly, the depth-resistivity models are depicted in Figure (B) for the combinations of F-F, C-F, F-M, C-M, F-VC, and C-VC.

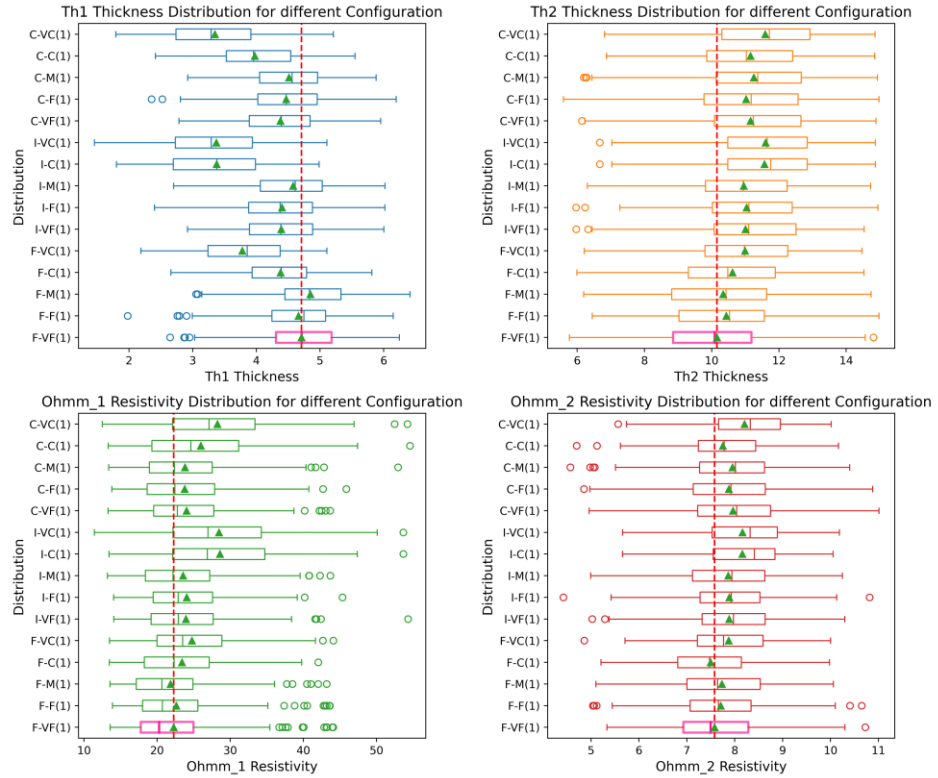


Figure 8: Box plot of first two thickness and resistivity. With one 1 iteration. Red line shows the benchmark F-VF(1). (1) represents the 1st iteration

Figure 8 shows the boxplot results for BEL1D-T with the threshold 0.135 for various combination of the discretization and can be compared to the corresponding solution with BEL1D-IPR (Figure 6). Differences are less pronounced than with BEL1D-IPR. The F-VF and F-F and F-M discretization have similar posterior distributions as the reference for the thickness of the first two layers, while the uncertainty range for the resistivity is slightly underestimated. Figure 6 shows that F-VF and F-F and F-M discretization lead to results without bias for any parameters.

As with BEL1D-IPR, the very coarse and coarse discretization are systematically biased. Most other combinations show a slight bias for the thickness of layer 2, and some also for layer 1. Interestingly, the difference with the reference for many combinations is less pronounced than for BEL1D-IPR. For example, the I-M and C-M combinations are giving relatively good approximations of the posterior. As in BEL1D-IPR the prior distribution is complemented with models sampled at the first iteration, without relying on their RMSE, an initial bias resulting from an error in the forward solver might be amplified in later iterations, leading to larger discrepancy between the response of final model and the data. With BEL1D-T, the application of the threshold after iteration 1 prevents the solution to deviate too much from the truth.

4.3. Impact of the Prior

In this section, we present some results obtained from the application of BEL1D to the TEM-fast dataset collected at sounding 2611, near project 22 (Figure 4). The measured signal can be seen in Figure 9, together with the standard deviation of the stacking error. A deterministic inversion of the data was carried out with SimPEG to have a first estimate of the electrical resistivity distribution (Figure 9). It shows a conductive zone at shallow depth, likely corresponding to the saline part of the unconsolidated aquifer, while more resistive ground is found below 15 meters, likely corresponding to the transition to the resistive bedrock. Below a gradual decrease of resistivity can be observed.

In field cases, defining the prior distribution can be complicated as the resistivity is not known in advance. We compare three possible prior combinations (obviously-inconsistent prior range - case A, slightly-inconsistent prior range case B, acceptable prior range - case C) to better understand the impact of the choice of the prior. We apply BEL1D-T to bypass the additional computational time required in BEL1D-IPR, and use the F-F discretization.

The prior model consists of 6 layers: the first five layers are characterized by their thickness and electrical resistivity, while the last layer has an infinite thickness. The prior distributions are shown in Figure 9 and Table 5. In case A, the prior is narrow and was chosen to represent the main trend observed in the deterministic inversion. However, the first layers (upper 10 m) have a small resistivity range not in accordance with the deterministic inversion (red line in Figure 9). Similarly, the fourth layer underestimates the range of resistivity expected from the deterministic inversion (60-70 Ohm.m). The prior for case B displays larger uncertainty: the first layer is forced to have larger resistivity values and a strong transition is forced for the half-space. Finally, the last prior case C is very wide and allows a large overlap between successive layers as well as a very large range of resistivity values.

Table 6: Prior distributions for the different cases a) Obviously inconsistent prior range, b) Slightly inconsistent prior range and c) Acceptable prior range.

	Case A		Case B		Case C	
	Thickness	Resistivity	Thickness	Resistivity	Thickness	Resistivity
	(m)	(ohmm)	(m)	(ohmm)	(m)	(ohmm)
Layer 1	0 – 10	2 – 5	0 – 10	10 – 25	0 – 10	10 – 55
Layer 2	5.0 – 10	0.5 – 6	5 – 10	0.5 – 5	5.0 – 10	0.5 – 15
Layer 3	0.5 – 10	20 – 100	0.5 – 10	20 – 50	0.5 – 10	20 – 100
Layer 4	35 – 50	60 – 70	35 – 50	50 – 100	35 – 50	50 – 600
Layer 5	45 – 60	5 – 10	45 – 60	0.2 – 0.5	45 – 60	0.2 – 10
layer 6	0 – 0	10 – 15	0 – 0	10 – 40	0 – 0	5 – 100

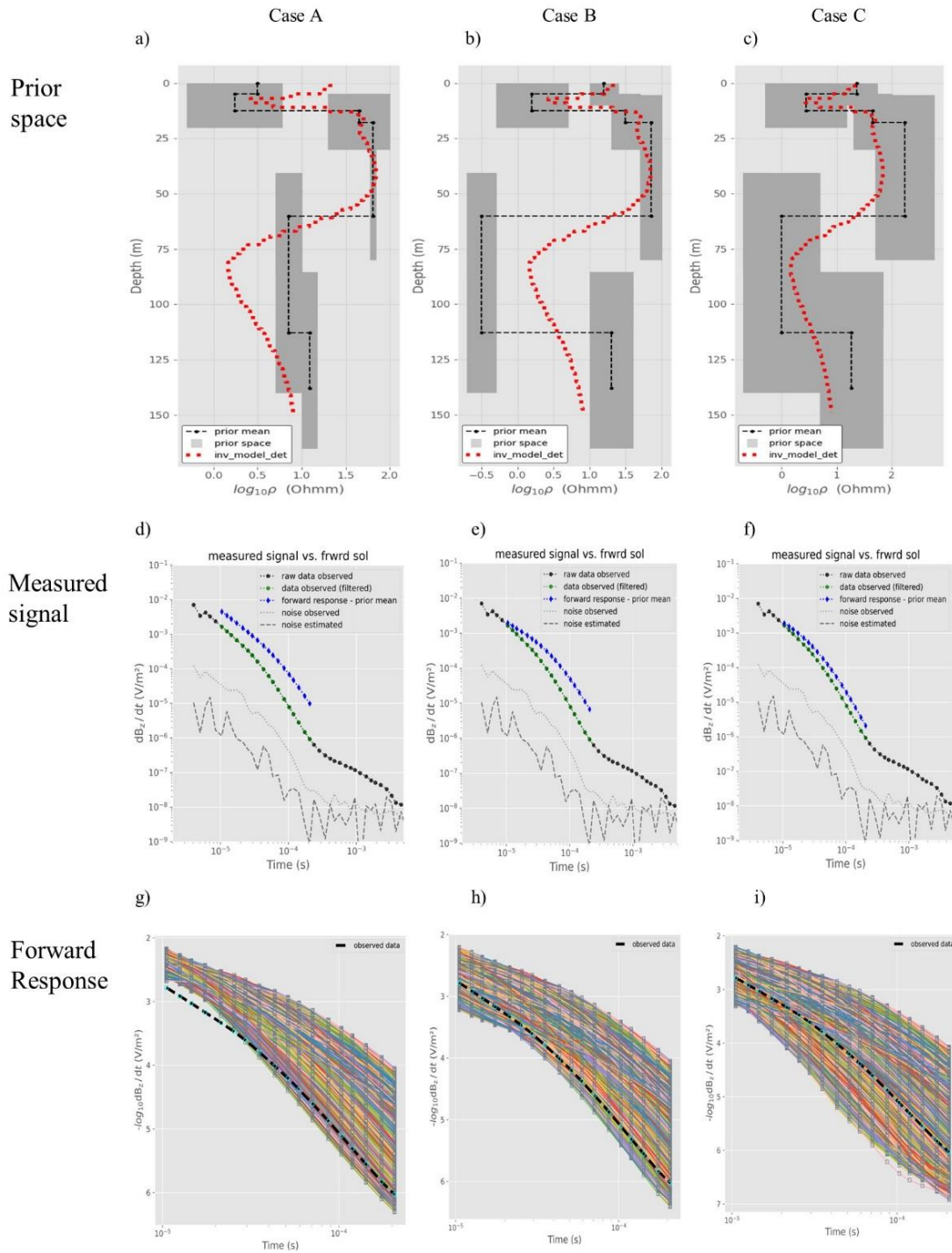


Figure 9: Prior distributions for the three cases of sounding 2611. Case A: Obvious inconsistent prior range, Case B : Slightly inconsistent prior range. Case C: Acceptable prior range. a-c) prior range with deterministic inversion (red), d-f) measured signal, noise and forward solution for the prior mean, g-i) forward response of each prior model.

The forward responses of the mean prior model of each three cases are displayed in Figures 9d to 9f. We can see that the response of the prior: (1) largely deviates from the measured signal for case A, (2) it deviates at later times for case B, and (3) it has the lowest deviation in case C. We also display the range of the forward response for 4000 prior models (Figure 9g to 9i). Due to the poor selection of the prior, a large difference between the measured data and the prior data space can be seen for case A (Figure 9g). The prior is clearly not consistent with the data as the latter lies outside of the prior range in the data space in the early time steps. On the other hand, for case B (Figure 9h), the prior data range now encompasses the observed data, although it is rather at the edge of the prior distribution. For case C (Figure 9i), the prior range in data space encompasses the measured data which lies close to the response of the prior mean model Figure 9f.

However, visual inspection is not sufficient to verify the consistency of the prior. Indeed, it is necessary to ensure that specific behaviors of the measured data can be reproduced by the prior model. This can be done more efficiently in the reduced PCA and CCA space [12,40]. Indeed, as BEL1D relies on learning, it cannot be used for extrapolation, and should not be used if the data falls outside of the range of the prior. To further support the argument, the PCA and (part of) the CCA spaces are shown in Figures 12 and 13 respectively. In Figure 12, the red crosses show the projection of the field data on every individual PCA dimension. It confirms that the prior for case A is inconsistent, with dimensions 2 and 3 lying outside, whereas the first PCA score lies at the edge of the prior distribution. For higher dimensions, the observed data lies within the range of prior data space, but those dimensions represent only a limited part of the total variance. This is an indication that the prior is not able to reproduce the data and is therefore inconsistent. For cases B and C, no inconsistency is detected in the PCA space.

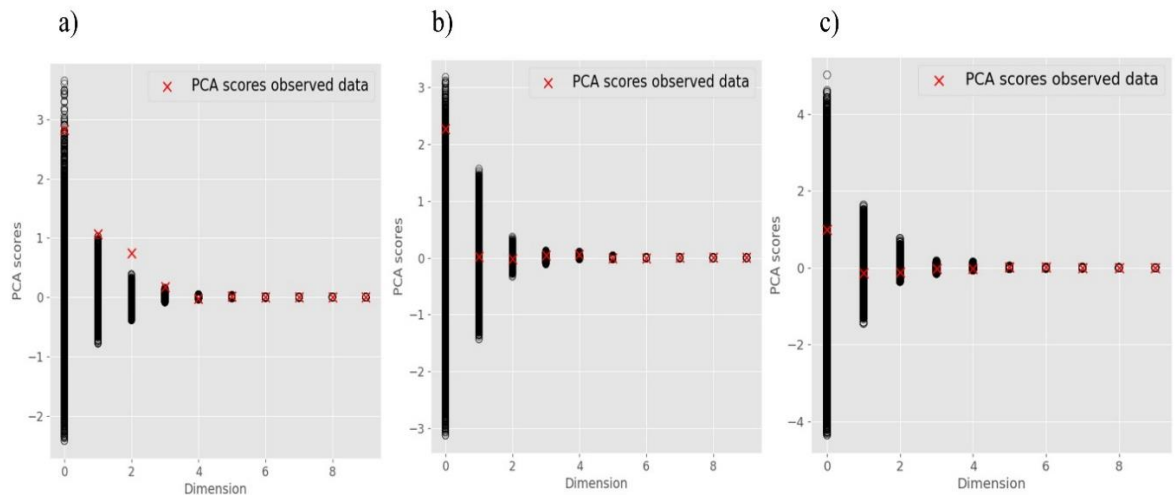


Figure 12: PCA space, a) Obvious inconsistent prior, b) Slightly inconsistent prior and c) Acceptable prior-. Black dot represents the prior models and the red cross represents the observed data.

A similar exercise is then performed in the CCA space where the projection of the field data is marked by a red line. In Figure 13(a) the observed data (red line) is lying outside of the zone covered by the sampled prior models for most dimensions (grey zone). In such a case BEL1D returns an error message and does not provide any estimation of the posterior. For the sake of illustration, we deactivated this preventive action and nevertheless performed the inversion. The posterior models in (Figure 14 (case A) shows low uncertainty for layer 1,2,4,5 and 6, because of the limited range provided in the prior. The posterior data space shows that the posterior models do not fit the data, as a result of the inability of BEL to extrapolate in this case. Note that the threshold was not applied in this case, as it would have left no sample in the posterior, since none of them fit the observed data.

For case B, although it is apparently consistent in the PCA space, a similar occurrence of inconsistency appears in the CCA space (Figure 13b) for dimension 3 and some higher dimensions. Although apparently consistent with each individual dimension, the observed data do not correspond to combinations of dimensions contained in the prior, in which case it constitutes an outlier for the proposed prior identified in the CCA space. However, in this case, the posterior models that are generated fit the data and have a relatively low RMSE (Figure 14c and 14d). The posterior model visualization shows a limited uncertainty reduction for layers 1 to 3 and almost no uncertainty reduction for layers 4, 5 and 6 (Figure 14c and 14d), likely pointing to a lack of sensitivity of the survey to these deeper layers. This indicates that BEL1D-T can overcome some inconsistency between the prior definition and the observed data, likely because the affected dimensions are only responsible for a small part of the total variance, to a level relatively similar to the noise level.

In case C, no inconsistency is detected in the prior data space, PCA and CCA space (Figure 12c, Figure 13c). The posterior models do fit the data within the expected noise level and the deterministic inversion lies within the posterior (Figure 14e and 14f). The posterior uncertainty is large, especially for deeper layers (4, 5 and 6). Therefore, in this case, BEL1D-T seems to correctly identify the posterior distribution of the model parameters. As the late times were filtered out, the data set is more sensitive to the shallow layers, and insensitive to the deeper layers. Increasing the prior range for those layers would also induce an increase of uncertainty in the posterior model.

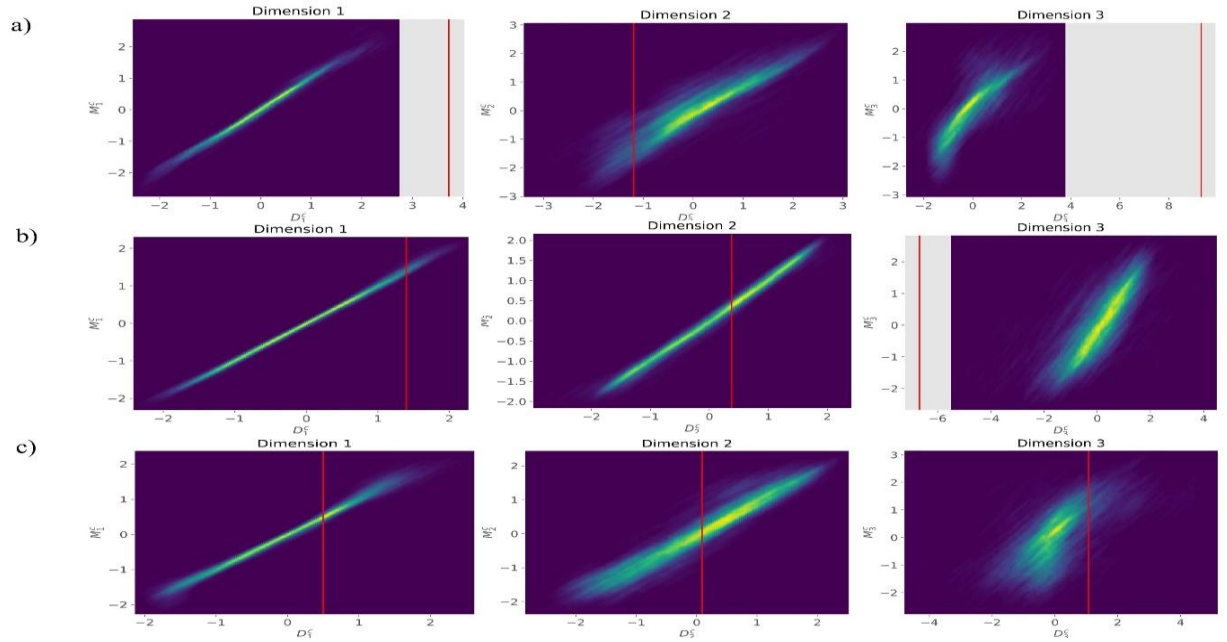
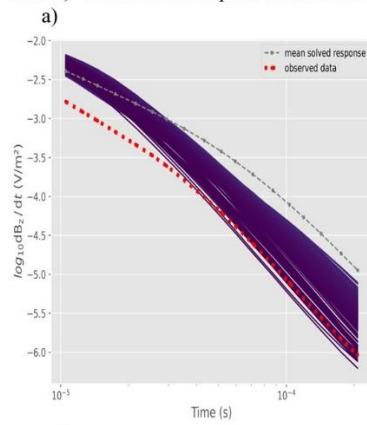
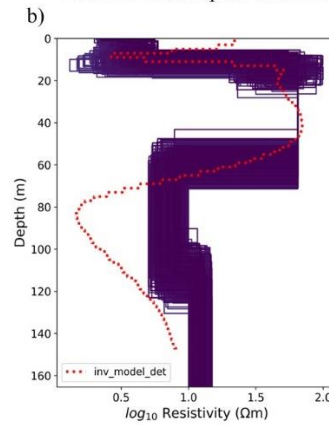


Figure 13: CCA space for the three first dimension, a) Obviously inconsistent prior, b) Slightly inconsistent prior and c) Acceptable prior. The red line represents the observed data. The y- axis corresponds to the reduced models and the x-axis corresponds to the reduced data.

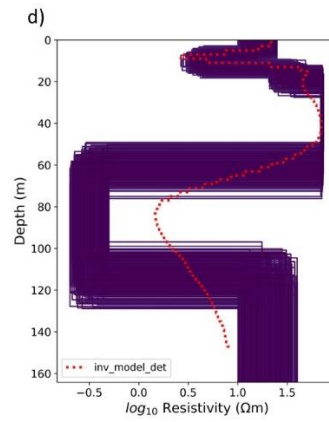
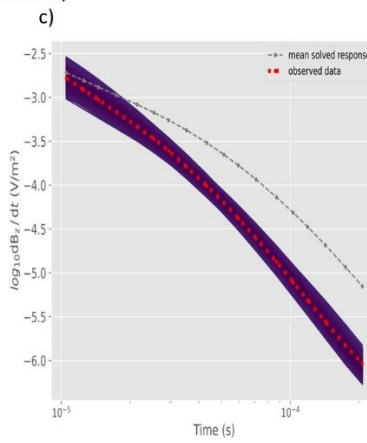
Case A) Posterior data space visualization



Posterior Model space visualization



Case B)



Case C)

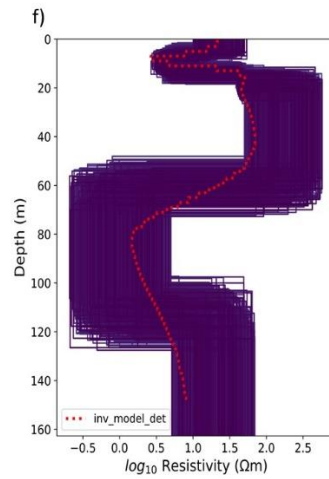
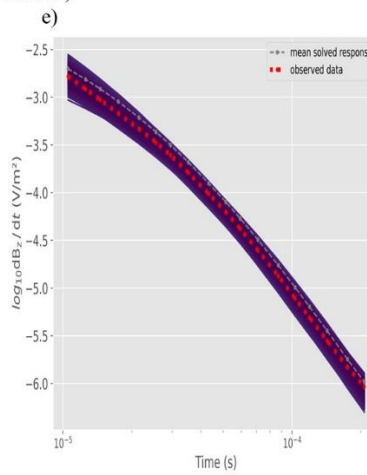


Figure 14: Response of both posterior data and /model space for the three prior selection. a-b) Obviously inconsistent prior range (without application of the threshold) c-d) Slightly inconsistent prior, e-f) Acceptable prior range.

4.4. Field soundings

We selected two TDEM soundings that are co-located with ERT profiles (red and yellow dots on Figure 4). The comparison with independent data can be used to evaluate the posterior solution from BEL1D-T. For the TDEM soundings (see figure 15c and 15d), we compare the deterministic inversion, the BEL1D-T posterior distribution and a conductivity profile extracted from the ERT profile at the location of the sounding.

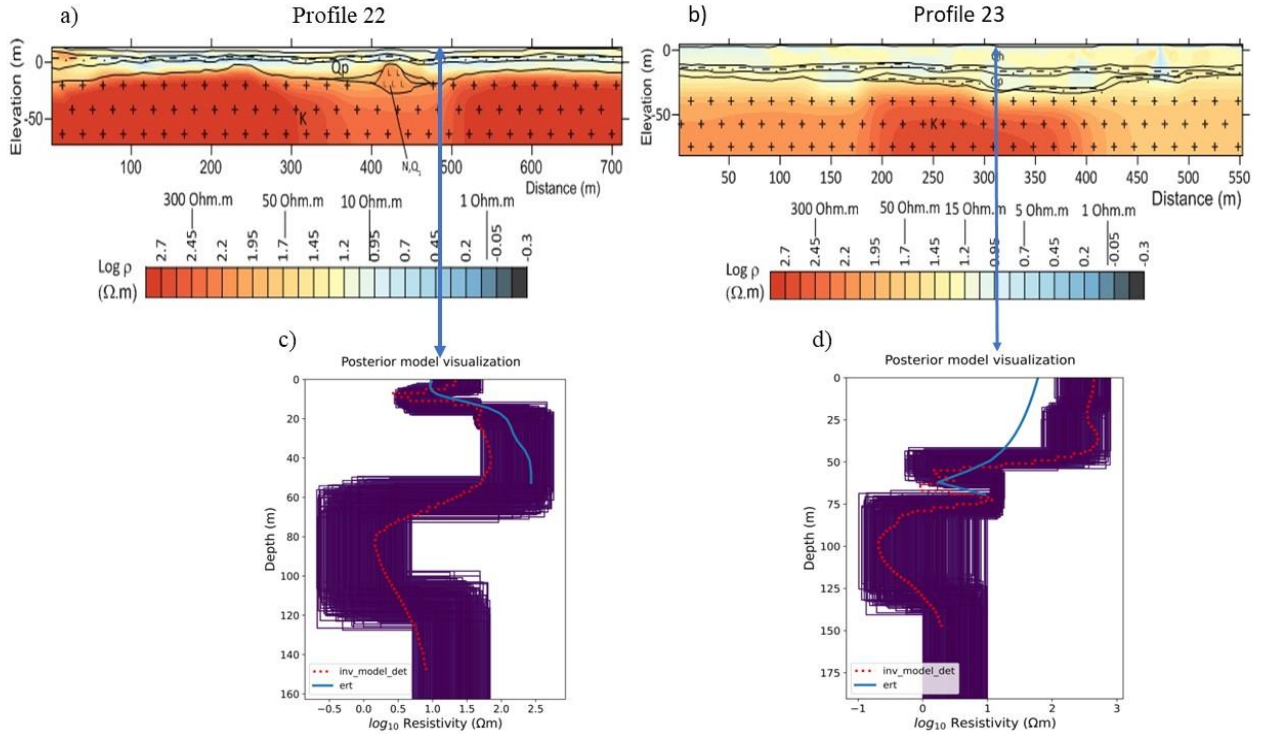


Figure 15: a) ERT profile 22 near to the Luy river b) ERT profile 23 near the dunes. Posterior model visualization for TDEM soundings on profile 22 (c) and 23 (d) ERT inversion in blue and deterministic inversion of TDEM data in red.

The resistivity image and TDEM results of profile 22 show the same trend (figure 15a and c). At shallow depth between 5 and 15 meters, less resistive layers are observed which indicate the presence of saltwater in the unconsolidated sediment (20 to 25m thickness). At larger depth, we have an increase in resistivity corresponding to the transition to the bedrock. The deterministic solution tends to show a decrease of resistivity at larger depths, which may be an artifact due to the loss of resolution. BEL1D-T is successful in providing a realistic uncertainty quantification compared to the deterministic inversion. It can be observed that except for the shallow layer, the reduction of uncertainty compared to the prior is relatively limited and concerns mostly the thickness and not the resistivity, illustrating the insensitivity of the

survey set-up for depths below 60 m where, the solution is mostly driven by the definition of the prior distribution. The selection of a rRMSE threshold however ensures that all those models are consistent with the recorded data.

The results for profile 23 are different (figure 15b and d). This site is at the foot of sand dunes, close to the sea, which have an elevation level between 11 and 50 m. The shallow layer is relatively resistive, but the two methods do not agree on the value of resistivity, with the TDEM resulting in higher values. Interestingly, BEL1D-T tends to predict a larger uncertainty towards low values of the resistivity for the shallow layers compared to the deterministic inversion. Below 50 m, the resistivity drops to 1-10 Ohm.m for both methods which seems to show the presence of saltwater in the bed rock. The uncertainty range estimated by BEL1D-T seems to invalidate the presence of rapidly varying resistivity between 50 and 75 m, predicted by the deterministic TDEM inversion, which is quite coherent with the lack of sensitivity at this depth.

4.5 Summary

Deterministic inversions are affected by the non-uniqueness of the solution preventing the quantification of uncertainty. Our approach using BEL1D-T allows us to retrieve not only the changes of resistivity with depth, but also to quantify the reliability of the model. We summarize the main outcomes of the sections above as:

1. When using a numerical forward model, the temporal and spatial discretization have a significant effect on the retrieved posterior distribution. The use of a semi-analytical approach is recommended when possible. Otherwise, BEL1D-T constitutes an efficient and fast alternative.
2. BEL1D-T is an efficient and accurate approach to predict uncertainty with a limited computational effort. It was shown to be equivalent to BEL1D-IPR but requires less forward models to be computed.
3. As any Bayesian approach, BEL1D-related methods are sensitive to the choice of the prior model. The consistency between the prior and the observed data is integrated, and the threshold approach allows to quickly identify inconsistent posterior model. We recommend to run a deterministic inversion to define the prior model, while keeping a wide range for each parameter allowing for sufficient variability.
4. For the field case, the results are consistent with ERT and deterministic inversion. our analysis reveal that the uncertainty reduction at depth greater than 60 m is almost non-existent. It is recommended to avoid the interpretation of the model parameters at that depth as the solution is likely highly dependent on the prior.

Conclusion

In this paper, we introduce a new approach combining BEL1D with a threshold after the first iteration (BEL1D-T) as a fast and efficient stochastic inversion method for TDEM data. Although BEL1D-T only requires a limited number of forward runs, the computational time remains relatively important as we used the numerical solver of SimPEG to calculate the forward response. The proper selection of timesteps and space discretization is essential to limit the computation cost while keeping an accurate solution. From our synthetic case, a threshold exists to avoid inducing an error in the estimation of the posterior distribution. If a relatively fine temporal discretization is required, especially during the early time-steps, a very fine spatial discretization does not seem mandatory. As this analysis is likely specific to every acquisition set-up and prior distribution, we suggest to carefully assess the modeling error introduced by the forward model before starting the BEL1D-T inversion. The use of faster semi-analytical forward models is recommended when available. However, 2D and 3D effects when 1D forward solver are used, are expected to have a similar impact on the forward model error as observed in our work.

The application of a threshold on the RMSE after one iteration is an efficient approach to limit the computational costs. We showed that selecting a threshold based on the expected noise level leads to a solution similar to the one obtained with the reference. The proposed approach allows to partly mitigate the adverse effects of an inaccurate forward models and therefore can be used to obtain a first fast assessment of the posterior distribution.

Moreover, it should be noted that, as with any stochastic methods, BEL1D is sensitive to the definition of the prior. We have experienced that some prior distributions that might appear visually consistent in the data space would result in inconsistencies in the low dimensional spaces. It is thus crucial to verify the consistency of the prior, also in the lower dimensional space. This feature is included by default in the pyBEL1D code (Michel, 2022), but it might be interesting to deactivate this feature in order to investigate the reasons and their impacts on the posterior. Beside the definition of the prior itself, the inconsistency can be attributed to the noisy nature of the field data [14].

In case of large uncertainty, an iterative prior resampling approach is advised as proposed by [14], but it comes at a larger computational cost. Therefore, we propose to reduce the prior uncertainty by using the deterministic inversion as a guide, and to limit ourselves to the first iteration, while filtering the models based on their RMSE. Doing this, BEL1D-T acts more as a stochastic optimization algorithm only providing a fast approximation of the posterior distribution, but still allowing to roughly estimate the uncertainty of the solution, without requiring heavy computational power such as HPC facilities.

We validated the approach using TDEM soundings acquired in a saltwater intrusion context in Vietnam. The posterior distribution was consistent with both the deterministic inversion and ERT profiles. The range of uncertainty was larger where TDEM and ERT deterministic inversions do not agree, which illustrate the intrinsic uncertainty of these type of data and the need for uncertainty quantification.

Supplementary Materials:

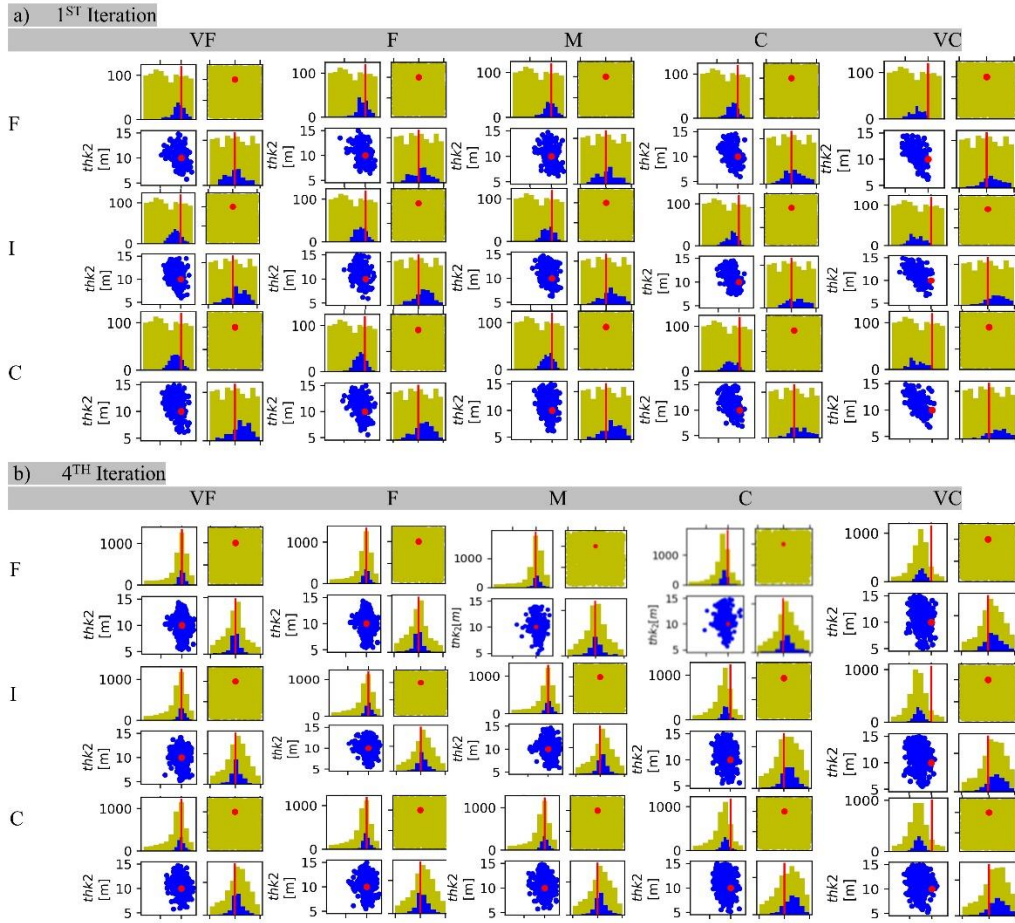


Figure A: a) Posterior model space visualization with one iteration and threshold (0.135), b) Posterior model space visualization with 4 iteration, the above row is with fine time discretization whereas the other rest of the rows are with intermediate and coarse time discretization. From the left to right with spatial discretization (VF, F, M, C, VC).

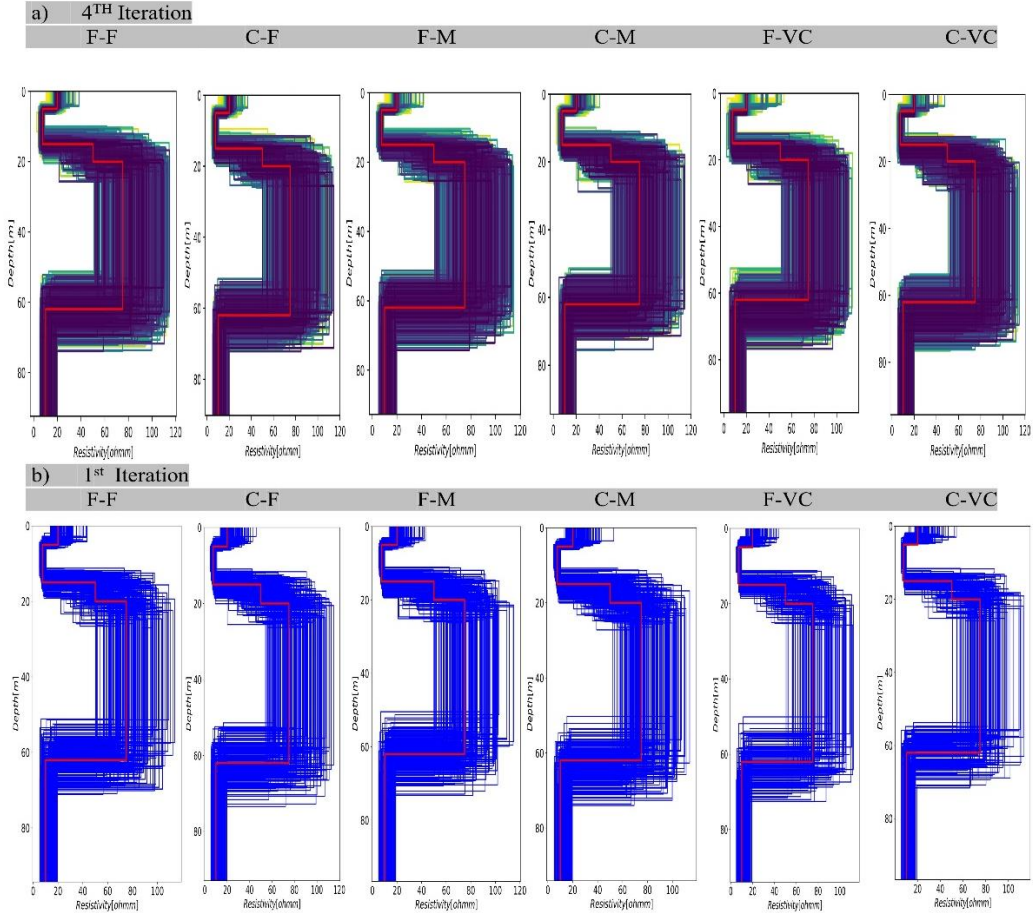


Figure B: Posterior model visualization *w.r.t* Depth (*m*) vs Resistivity (*ohmm*), color bar represents the RMSE values, a) with four iteration without threshold and b) with one iteration and a 0.135 threshold value.

The depth-resistivity models are shown in Figure (B). Although more difficult to interpret, they look very identical. The F-F and F-M combinations are nearly identical to the reference, while the C-F and C-M only overestimates slightly the range for the thickness of the first layer. A bias can be recognized in the combinations F-VC and C-VC when comparing the posterior with the reference, in particular at the 15 m depth transition corresponding to an increase in resistivity, and similarly for the transition to the half-space. Similar trend can be observed for the solution after 1 iteration and a threshold of 0.135.

Author Contributions: The conceptualization of this project was led by TH, with contribution of AA, DD and AFO. The methods were developed by HM (implementation of BEL1D and BEL1D-IPR), AA (BEL1D-T link SimPEG forward solver), LA and WD (link SimPEG forward solver with BEL1D-IPR). AA ran all simulations (discretization, threshold, prior selection, field data). The initial draft was written by AA with significant input from TH. All authors edited and reviewed the draft. TH and DD provided supervision for AA throughout the whole research. Project administration: TH and Funding acquisition: AA, TH.

Funding:

AA, received funding from the Higher Education Commission (HEC) of Pakistan between 2019 and 2023, with reference number 5-1/HRD/UESTP1(Batch-IV)/84545/2019/HEC, and from the Bijzonder Onderzoeksfonds (BOF) of Ghent University, with grant number BOF.CDV.2023.0058.01. WD, was funded by the Fund for Scientific Research (FWO) in Flanders, with grants 1113020N and 1113022N and Postdoctoral Mandate PDMt223065. HM was funded by the F.R.S.-FNRS, with grants 32905391 and 40000777.

Data Availability Statement: The field data can be made available upon request.

Acknowledgments: We thank Robin Thibaut for helping in the analysis and plotting of the PCA space. We thank Robin Thibaut, Linh Pham Dieu, Diep Cong-Thi and all the team from the VIGMR for field data collection.

Conflicts of Interest: The authors declare no conflicts of interest.

References

1. Kemna, A., Nguyen, F., Gossen, S., 2007. On linear model uncertainty computation in 1.electrical imaging. In: Presented at the SIAM Conference on Mathematical and Computational Issues in Geosciences. Santa Fe.
2. Hermans, Thomas; Vandenbohede, Alexander; Lebbe, Luc; Nguyen, Frédéric (2012). *A shallow geothermal experiment in a sandy aquifer monitored using electric resistivity tomography*. *GEOPHYSICS*, 77(1), B11–B21. doi:10.1190/geo2011-0199.1
3. Parsekian, A. D., & Grombacher, D. (2015). Uncertainty estimates for surface nuclear magnetic resonance water content and relaxation time profiles from bootstrap statistics. *Journal of Applied Geophysics*, 119, 61-70.
<https://doi.org/10.1016/j.jappgeo.2015.05.005>
4. Aster, R., Borchers, B., Thurber, C., 2013. *Parameters Estimation and Inverse Problems*, second ed. Academic Press.
5. Sambridge, M., 2002. Monte Carlo methods in geophysical inverse problems. *Rev. Geophys.* 40 <https://doi.org/10.1029/2000RG000089>.
6. Irving, J., Singha, K., 2010. Stochastic inversion of tracer test and electrical geophysical data to estimate hydraulic conductivities. *Water Resour. Res.* 46 <https://doi.org/10.1029/2009WR008340>.
7. Trainor-Guitton, W., Hoversten, G.M., 2011. Stochastic inversion for electromagnetic geophysics: practical challenges and improving convergence efficiency. *Geophysics* 76, F373–F386. <https://doi.org/10.1190/geo2010-0223.1>.
8. De Pasquale, G.; Linde, N. (2017). On structure-based priors in Bayesian geophysical inversion. *Geophysical Journal International*, 208(3), 1342–1358. doi:10.1093/gji/ggw458
9. Ball, L. B., Davis, T. A., Minsley, B. J., Gillespie, J. M., & Landon, M. K. (2020). Probabilistic Categorical Groundwater Salinity Mapping From Airborne Electromagnetic Data Adjacent to California’s Lost Hills and Belridge Oil Fields. *Water Resources Research*, 56(6). <https://doi.org/10.1029/2019WR026273>
10. Bobe, C., Hanssens, D., Hermans, T., Van De Vijver, E., 2020. Efficient Probabilistic Joint Inversion of Direct Current Resistivity and Small-Loop Electromagnetic Data. *Algorithms* 13, 144. <https://doi.org/10.3390/a13060144>
11. Tso, C.-H.M., Iglesias, M., Wilkinson, P., Kuras, O., Chambers, J., Binley, A., 2021. Efficient multiscale imaging of subsurface resistivity with uncertainty quantification using ensemble Kalman inversion. *Geophysical Journal International* 225, 887–905. <https://doi.org/10.1093/gji/ggab013>

12. Hermans, T., Nguyen, F., Klepikova, M., Dassargues, A., Caers, J., 2018. Uncertainty quantification of medium-term heat storage from short-term geophysical experiments using bayesian evidential learning. *Water Resour. Res.* 54, 2931–2948. <https://doi.org/10.1002/2017WR022135>.
13. Michel, H., Hermans, T., Kremer, T., Elen, A., Nguyen, Fr  e., 1D geological imaging of the subsurface from geophysical data with Bayesian Evidential Learning. Part 2: Applications and software, *Computers and Geosciences* (2020), doi: <https://doi.org/10.1016/j.cageo.2020.104456>.
14. Michel, H., Hermans, T., & Nguyen, F. (2023). Iterative Prior Resampling and rejection sampling to improve 1D geophysical imaging based on Bayesian Evidential Learning (BEL1D). *Geophysical Journal International*, 232 (2), 958–974. <https://doi.org/10.1093/GJI/GGAC372>
15. Kremer, T., M  ller-Petke, M., Michel, H., Dlugosch, R., Irons, T., Hermans, T., Nguyen, F., 2020. Improving the accuracy of 1D surface nuclear magnetic resonance surveys using the multi-central-loop configuration. *Journal of Applied Geophysics* 177, 104042.
16. Heagy, Lindsey J.; Cockett, Rowan; Kang, Seogi; Rosenkjaer, Gudni K.; Oldenburg, Douglas W. (2017) . *A framework for simulation and inversion in electromagnetics. Computers & Geosciences*, (), S0098300416303946-.doi:10.1016/j.cageo.2017.06.018
17. Siemon, B., Christiansen, A. V., & Auken, E. (2009). A review of helicopter-borne electromagnetic methods for groundwater exploration. *Near Surface Geophysics*, 7(5–6), 629–646. <https://doi.org/10.3997/1873-0604.2009043>
18. Vilhelmsen, T., Marker, P., Foged, N., Wernberg, T., Auken, E., Christiansen, A.V., Bauer-Gottwein, P., Christensen, S., H  yer, A.-S., 2018. A Regional Scale Hydrostratigraphy Generated from Geophysical Data of Varying Age, Type, and Quality. *Water Resources Management*. <https://doi.org/10.1007/s11269-018-2115-1>
19. Goebel, M., Knight, R., Halkj  r, M., 2019. Mapping saltwater intrusion with an airborne electromagnetic method in the offshore coastal environment, Monterey Bay, California. *Journal of Hydrology: Regional Studies* 23, 100602. <https://doi.org/10.1016/j.ejrh.2019.100602>
20. Auken, E., Foged, N., Larsen, J. J., Lassen, K. V. T., Maurya, P. K., Dath, S. M., & Eiskj  r, T. T. (2019). tTEM — A towed transient electromagnetic system for detailed 3D imaging of the top 70 m of the subsurface. *Geophysics*, 84(1), E13–E22. <https://doi.org/10.1190/geo2018-0355.1>
21. Lane, J. W., Jr, Briggs, M. A., Maurya, P. K., White, E. A., Pedersen, J. B., Auken, E., Terry, N., Minsley, B., Kress, W., LeBlanc, D. R., Adams, R., & Johnson, C. D. (2020). Characterizing the diverse hydrogeology underlying rivers and estuaries using new floating transient electromagnetic methodology. *The Science of the Total Environment*, 740(140074), 140074. <https://doi.org/10.1016/j.scitotenv.2020.140074>
22. Aigner, L., H  genauer, P., B  cker, M., & Flores Orozco, A. (2021). A flexible single loop setup for water-borne transient electromagnetic sounding applications. *Sensors*, 21(19), 6624.

23. Bucker, M., Flores Orozco, A., Gallistl, J., Steiner, M., Aigner, L., Hoppenbrock, J., ... & Pérez, L. (2021). Integrated land and water-borne geophysical surveys shed light on the sudden drying of large karst lakes in southern Mexico. *Solid Earth*, 12(2), 439-461.
24. Viezzoli, A., Christiansen, A. V., Auken, E., & Sørensen, K. (2008). Quasi-3D modeling of airborne TEM data by spatially constrained inversion. *GEOPHYSICS*, 73(3), F105–F113. <https://doi.org/10.1190/1.2895521>
25. Michel, H. (2022). *pyBEL1D: A Python implementation of BEL1D* (1.1.0). <https://doi.org/10.5281/ZENODO.6833249>
26. Hermans, T., Oware, E., Caers, J., 2016. Direct prediction of spatially and temporally varying physical properties from time-lapse electrical resistance data. *Water Resources Research* 52, 7262–7283. <https://doi.org/10.1002/2016WR019126>
27. Krzanowski, W.J., 2000. Principles of multivariate analysis: a user's perspective. In: Oxford Statistical Series, Revised Edition. Oxford University Press, New York
28. Wand, M.P., Jones, M.C., 1993. Comparison of smoothing parameterizations in bivariate kernel density estimation. *J. Am. Stat. Assoc.* 88, 520. <https://doi.org/10.2307/2290332>.
29. Devroye, Luc. (1986). An Automatic Method for Generating Random Variates with a Given Characteristic Function. *SIAM Journal on Applied Mathematics*, 46(4), 698–719. doi:10.1137/0146046
30. Werthmüller, D. (2017) An open-source full 3D electromagnetic modeler for 1D VTI media in Python: Empymod. *Geophysics* 2017, 82, WB9–WB19. doi: 10.1190/geo2016-0626.1
31. Yee, K. (1966). Numerical solution of initial boundary value problems involving maxwell's equations in isotropic media. *IEEE Transactions on Antennas and Propagation*, 14(3), 302–307. <https://doi.org/10.1109/tap.1966.1138693>
32. R. Cockett; S. Kang; L. J. Heagy; A. Pidlisecky; D. W. Oldenburg (2015). *SimPEG: An open source framework for simulation and gradient based parameter estimation in geophysical applications.* , (), -. doi:10.1016/j.cageo.2015.09.015
33. Haber, E., 2014. Computational Methods in Geophysical Electromagnetics. Society for Industrial and Applied Mathematics, Philadelphia, PA. URL <http://epubs.siam.org/doi/book/10.1137/1.9781611973808>.
34. Hyman, J., Morel, J., Shashkov, M., Steinberg, S., 2002. Mimetic finite difference methods for diffusion equations , 333–352.
35. Hyman, J. M., Shashkov, M., 1999. Mimetic Discretizations for Maxwell s Equations 909, 881–909.
36. Diep Cong-Thi;Linh Pham Dieu;Robin Thibaut;Marieke Paepen;Huu Hieu Ho;Frédéric Nguyen;Thomas Hermans; (2021). Imaging the Structure and the Saltwater Intrusion Extent of the Luy River Coastal Aquifer (Binh Thuan,

Vietnam) Using Electrical Resistivity Tomography . Water, (), –
. doi:10.3390/w13131743

37. Dieu, L.P.; Cong-Thi, D.; Segers, T.; Ho, H.H.; Nguyen, F.; Hermans, T. Groundwater Salinization and Freshening Processes in the Luy River Coastal Aquifer, Vietnam. *Water* **2022**, *14*, 2358. <https://doi.org/10.3390/w14152358>
38. Paepen, M.; Hanssens, D.; De Smedt, P.; Walraevens, K.; Hermans, T. Combining resistivity and frequency domain electromagnetic methods to investigate submarine groundwater discharge (SGD) in the littoral zone. *Hydrol. Earth Syst. Sci.* 2020.
39. Paepen, M., Deleersnyder, W., De Latte, S., Walraevens, K., Hermans, T., 2022. Effect of Groundwater Extraction and Artificial Recharge on the Geophysical Footprints of Fresh Submarine Groundwater Discharge in the Western Belgian Coastal Area. *Water* *14*, 1040. <https://doi.org/10.3390/w14071040>
40. Hermans, T., Lesparre, N., De Schepper, G., Robert, T., 2019. Bayesian evidential learning: a field validation using push-pull tests. *Hydrogeol J* *27*, 1661–1672. <https://doi.org/10.1007/s10040-019-01962-9>
41. Haber, Elda. 2014. *Computational Methods in Geophysical Electromagnetics*. SIAM, 62-67. <http://books.google.ca/books?id=favjoQEACAAJ>